Femtosecond temporal probes using spectrally tailored noisy quasi-cw laser light

Dirk C. DeMott, Darin J. Ulness, and A. C. Albrecht
Department of Chemistry, Cornell University, Ithaca, New York 14853-1301
(Received 20 February 1996)

Theory and experiment are presented that suggest a new avenue for designing femtosecond temporal probes in which multiple spatially overlapped noisy (nontransform limited) quasi-cw laser light beams are tailored in a controllable fashion by dispersion. The generation of femtosecond probes is demonstrated experimentally by combining the output from two distinct nanosecond pulsed dye lasers to form a single ''tailored'' beam having a double-peaked spectral density corresponding to the superposition of emission spectra of each of the dye lasers. The interferograms produced from this single beam display features on the time scale significantly shorter than the autocorrelation time of either of the component beams alone. The theory, incorporating controllable dispersion effects, correctly captures the interferometric patterns seen in noisy light two-color frequency summing experiments and is general enough to treat experiments involving the spatially combined emission of an arbitrary number of light sources. Concepts both of noisy light spectroscopy and of amplitude modulated pulse shaping are applied. Applications of such tailored noisy light sources to wave-packet preparation and even photochemical control may be anticipated. [S1050-2947(97)02101-X]

PACS number(s): 42.65.Re, 42.50.Md

I. INTRODUCTION

For some time it has been known that femtosecond scale molecular dynamics can be probed by laser pulses of long duration provided the light is noisy[1] and possesses sufficient bandwidth to have an autocorrelation time on the femtosecond time scale [1]. The noisy light has an autocorrelation time similar to the autocorrelation time of transform limited light pulses of equivalent bandwidth although the noisy light can, in principle, be cw.

Noisy light interferometry may be introduced into any or all of the optical spectroscopies—linear and nonlinear—to achieve time resolution comparable to that available with coherent femtosecond pulses [2]. Nevertheless these two light sources are different in two fundamental ways. First, the noisy source, though pulsed, is effectively nearly continuous (or quasi-cw) as well as more energetic than the femtosecond source, which is a true ultrashort pulse in time. In either case one must be careful not to overdrive a lossy sample (and thereby invalidate the perturbative approach to light-matter interaction). For the typical nanosecond noisy light pulse the total energy upon a sample usually exceeds that of a typical (amplified) femtosecond pulse by an order of magnitude. Thus, noisy light experiments must be relatively concerned about overdriving the sample at the linear level (bleaching, photochemistry, etc.), while in femtosecond work, where peak powers can exceed those of a noisy light source by orders of magnitude, one must be concerned about invalidating the perturbative approach at the nonlinear level. To date in applications of either method these distinct potential problems have been successfully circumvented (by controlling both the incident flux and degree of focusing). More fundamentally, the quasi-cw nature of the noisy light source inherently limits the dynamic range of noisy light interferometry. There is always a ''background'' signal. However, depending on the spectroscopy, this background can be several orders of magnitude weaker than the principal region of the interferogram, thus offering a dynamic range comparable to that of a femtosecond pulse [3].

A second fundamental distinction between the two kinds of sources concerns the concept of ''cross-color'' coherence. While both sources may share identically broad spectra, the fields from a noisy source possess random relative phases among the available colors. There is no cross-color coherence; the field correlators are ''color locked.'' A femtosecond pulse, whether chirped or truly transform limited, consists of fields characterized by nonrandom relative phases among the colors. As a consequence, the nature of their action on a material, and the dynamics that are probed, can differ in important, complementary ways. For example, it has been shown how in time-resolved coherent Raman spectroscopy [4] where the available spectral width can drive two Raman oscillators, the coherent femtosecond source provides only the beat frequency between the oscillators and the arithmetic mean of their vibrational dephasing rate constants. In contrast, because of color locking, noisy light interferometry (joined with a monochromatic field) having only a 2:1 dynamic range easily recovers both the Bohr frequency and the dephasing rate constant for each oscillator with high precision. Another interesting distinguishing example would appear in pump-probe femtosecond experiments—a standard method for probing ultrafast events with coherent femtosecond pulses. At the pump step the femtosecond source produces new state populations and (because of cross-color phase locking) vibrational wave packets can be created. The wave packets may appear in both the upper and in the lower electronic surface of the resonant chromophore. As the pump-probe time delay is increased Bohr frequency oscillations are seen in the probe signal that decays according to the vibrational coherence dynamics of the wave packet but is

[1]Here ''noisy'' is used to describe light, the frequency components of which have relative phases sufficiently indeterminate to be modeled using a noise function obeying complex Gaussian statistics.

also entangled with population decay. In the same experiment with noisy light the principal term involves a pump step that is not cross-color phase locked so it is unable to produce a coherent vibrational wave packet on an individual chromophore. Instead the pump step is color locked and will only leave a population in some vibrational state in the excited electronic state surface. However, since the probe step (heterodyned) may color lock on a different vibronic transition (or on the same one) the Bohr frequency is exposed as difference beats in the white detected interferogram. But it turns out that the decay of these oscillations will be a measure of the dynamics of the vibronic coherence prepared in the first half of the pump step (vibronic coherence times would be measured). It will not measure the vibrational coherence dynamics nor will the principal component of the signal be entangled with population decay as in the experiment with femtosecond pulses. Often vibronic dephasing times can be very short and may easily be less than the period of many low-frequency vibrational modes thus leaving their oscillations overdamped and undetected. However, larger vibrational frequencies, normally outside of the spectral reach of coherent femtosecond light, need not be overdamped. These can be studied using multicolored noisy light sources such as those presented in this paper. Finally, when the dynamics of polyatomic chromophores are the subject of study their characteristic multilevel systems cause both experimental approaches to be entangled (but in different ways) with dynamics that can be more determined by the spectral width of the light than the molecule-bath interaction of interest.

It is becoming increasingly apparent that ultrafast measurements based on noisy light interferometry provide their own unique view of material dynamics. It is therefore useful to explore ways of tailoring new noisy light sources. Since such sources are not cross-color phase locked such tailoring can be relatively straightforward and, as we shall see, achieved simply by superposing sources derived from separate lasers. A review of many noisy light experiments with a discussion of the practical advantages and disadvantages has been given by Kobayashi [5].

It is shown here that when composite spectral densities are achieved by combining two or more nontransform limited quasi-cw[2] sources collinearly to form one beam, nonlinear autocorrelation interferograms are generated that exhibit fringes capable of better temporal resolution than possible from one noisy source alone. Recently [6] the first application of this capability has been demonstrated in a three-color interferometric coherent Raman scattering experiment where two of the colors are derived from a two-color tailored source such as that analyzed here. Sub-thirty femtosecond light-matter beats are seen where the autocorrelation time for each separate noisy light source exceeds 100 fs. In principle by tailoring spectra beyond simple broadband sources one can in fact customize the shape of the autocorrelation function at any order. Customized temporal probes have been demonstrated in the ultrashort pulse domain [7,8]. Pulse shaping with real femtosecond pulses involves programmable liquid-crystal arrays that modulate the amplitude and/or phase to produce tailored ultrashort pulses [9]. Such controllability should provide a sophisticated tool for selectively producing wave packets and driving photochemical reactions [7,5,10]. Both theory and experiment show that the tailored field can be used in the quantum control of matter [11]. It is possible that spectrally tailored quasi-cw light may provide another interesting approach to these problems—one that may have an advantage in terms of wavelength selection via the choice of laser dye. However, it appears that for fundamental reasons quasi-cw light is amenable to amplitude modulation but not to phase modulation. Nevertheless, as will be shown, a pseudo-phase modulation is available through experimental control of the unbalanced dispersion of the two arms of the interferometer, which is essential to noisy light experiments.

The demonstration experiment is based on a dual dye noisy light source with unbalanced dispersion effects for interferometric second-harmonic generation (called $I^{(2)}$SHG), or, preferably interferometric frequency summing, $I^{(2)}FS(2)$, since there are two distinct colors (carrier frequencies) involved.[3]

First, a somewhat general theoretical treatment is offered that properly captures the $I^{(2)}FS(2)$ signal as derived from tailored light composed of several quasi-cw sources. Afterwards the effects of unbalanced dispersion between the two arms of the Michelson interferometer are introduced to expose an additional method for tailoring the light field. Next, the general dual color noisy beam $I^{(2)}FS(2)$ experiment is outlined and experimental details for producing a series of dual color noisy light sources are presented. The observed $I^{(2)}FS(2)$ signal from three such tailored sources are presented and fit to theory in the section prior to concluding remarks.

II. THEORY

A simple theory can capture the essence of the observed $I^{(2)}FS(2)$ interferograms. The second-order electrical polarization, within the zero memory approximation (ZMA), is presented for light fields containing a complex noise function; the $I^{(2)}FS(2)$ interferogram (an intensity level signal) is expressed in terms of the resulting four-point time correlation functions for the noisy quasi-cw light. These are written in terms of stochastically averaged noise functions, which are reduced to products of pair correlators that themselves are Fourier transforms of the composite spectral density of the tailored source. The theory is extended to include effects of unbalanced dispersion within the two arms of the interferometer. Such differential dispersion effects prove to be significant and observable. Their control offers another tool for tailoring the structure of the interferogram.

A. The general $I^{(2)}FS(2)$ interferogram

For convenience, the theory is formulated for scalar fields $\mathbf{E}(\mathbf{r},t) \Rightarrow E(\mathbf{r},t)$. Consider a composite beam made of a su-

[2]The term ''quasi-cw'' is used because the pulse duration exceeds the femtosecond time scale of the interferogram by several orders of magnitude.

[3]The superscript (2) indicates that two interventions of the tailored field drive the nonlinear process, I stands for interferometric, and FS(2) indicates two-color frequency summing.

perposition of c separate quasi-cw light fields, referred to as component light fields, the jth having real amplitude E_j^0, a complex noise function $p_j(t)$, and a principal carrier frequency, ϖ_j. These light fields are thought to issue from separate lasers and are taken to be completely uncorrelated (other than the temporal overlap of their respective pulse envelopes). The composite (''tailored'') beam enters a Michelson interferometer where it is split into two beams. In one arm the composite field F is under fixed delay and is directed into a sample along a laboratory unit vector $\hat{\mathbf{e}}$. Thus the jth quasi-cw field component of F will have k vector $\mathbf{k}_j = k_j \hat{\mathbf{e}}$. In the second arm the composite field F' is subject to a variable delay τ relative to F by an amount τ, and is directed into the sample along a laboratory unit vector $\hat{\mathbf{e}}'$. The jth quasi-cw field component in F' has k vector $\mathbf{k}_j' = k_j' \hat{\mathbf{e}}'$.

The electric fields associated with F and F' are then

$$E_F(\mathbf{r},t) = \sum_j^c E_j^0 p_j(t) e^{ik_j \hat{\mathbf{e}}\cdot\mathbf{r} - i\varpi_j t} + \text{c.c.}, \tag{1}$$

and

$$E_{F'}(\mathbf{r},t) = \sum_j^c E_j^0 p_j(t-\tau) e^{ik_j' \hat{\mathbf{e}}'\cdot\mathbf{r} - i\varpi_j (t-\tau)} + \text{c.c.} \tag{2}$$

The complex noise functions (p_j's) that carry the noise associated with the complex fields are assumed to be stationary and ergodic (on the femtosecond time scale) and are taken to obey complex Gaussian statistics [12]. When these assumptions fail, alternative formulations of spectral tailoring based on nonstationary statistics or fully deterministic light fields become useful.

The mth-order macroscopic electric polarization for m-color frequency summing, FS(m), is given by [13]

$$P^{(m)}(\mathbf{r},t,\tau) \propto \int_{-\infty}^{\infty} d\omega_1 \cdots d\omega_m \chi^{(m)}(-\omega_\Sigma;\omega_1,\ldots,\omega_m) \tilde{E}(\mathbf{r},\omega_1)\cdots\tilde{E}(\mathbf{r},\omega_m) e^{-i\omega_\Sigma t}, \tag{3}$$

where $\omega_\Sigma \equiv \omega_1 + \cdots + \omega_m$ and $\tilde{E}(\mathbf{r},\omega_1)$ is the time transform of $E(\mathbf{r},t)$. Whenever the ZMA holds, $\chi^{(m)}$ is a slowly varying real function of frequency over the bandwidth of the light—hence it may be brought outside the integral as a constant, $\chi_{m\varpi}$. The second-order polarization ($m=2$) due to one action of F and one of F' [noncollinear FS(2)], becomes with Eqs. (1) and (2)

$$P_{\text{FS}}(\mathbf{r},t,\tau) \propto \chi_{2\varpi} \sum_k^c \sum_j^c \int_{-\infty}^{\infty} dq_j \int_{-\infty}^{\infty} dq_k E_j^0 E_k^0 \tilde{p}_j(q_j - \varpi_j)\tilde{p}_k(q_k - \varpi_k) e^{-i(q_j+q_k)t} e^{iq_k\tau} e^{i(k_j\hat{\mathbf{e}} + k_k'\hat{\mathbf{e}}')\cdot\mathbf{r}}, \tag{4}$$

where the $q_{j,(k)}$'s are dummy frequency variables centered about the nominal carrier frequencies, $\varpi_{j,(k)}$, of the component frequencies (n.b., when $j=k$ the q_k remain independently variable, so one is accented: $\dot{q}_j$ is distinct from q_j). The $\tilde{p}_j$'s are the Fourier transforms[4] of the p_j's. The new FS(2) field launched by the second-order polarization is $E_{\text{FS}}(t,\tau) \propto \int d\mathbf{r} e^{i\mathbf{k}_{jk}\cdot\mathbf{r}} P_{\text{FS}}(\mathbf{r},t,\tau)$. This leads to the phase-matching condition $\mathbf{k}_{jk} = k_j\hat{\mathbf{e}} + k_k'\hat{\mathbf{e}}'$, where $\mathbf{k}_{jk}$ is the signal k vector of the FS(2) field produced by the jth and kth component of the composite beam. It should be noted that the optimally phase-matched alignment of a summing crystal is different for different component color pairs, so one is forced experimentally to be satisfied with some compromise alignment. Collection of all the signal fields on the detector is, however, not a problem.

The phase-matched I$^{(2)}$FS(2) signal is detected (and stochastically averaged) at the intensity level. Its intensity becomes

$$I_{\text{FS}}(\tau,t) \propto \langle E_{\text{FS}}^*(\tau,t) E_{\text{FS}}(\tau,t)\rangle \propto \chi_{2\varpi}^2 \sum_k^c \sum_j^c \sum_l^c \sum_m^c \int_{-\infty}^{\infty} dq_j \int_{-\infty}^{\infty} dq_k \int_{-\infty}^{\infty} dq_l \int_{-\infty}^{\infty} dq_m E_j^0 E_k^0 E_l^0 E_m^0$$
$$\times \langle \tilde{p}_l^*(q_l - \varpi_l)\tilde{p}_m^*(q_m - \varpi_m)\tilde{p}_j(q_j - \varpi_j)\tilde{p}_k(q_k - \varpi_k)\rangle e^{i(q_k - q_m)\tau} e^{-i(q_j + q_k - q_l q_m)t}, \tag{5}$$

where the $\langle\ \rangle$ indicates a stochastic average over the noise. Since the $\tilde{p}_j$'s obey complex Gaussian statistics, the complex Gaussian moment theorem can be employed to break the four-point correlator in (5) into two terms, each containing a product of pair (two point) correlators. The four-point correlator becomes

$$\langle \tilde{p}_l^*(q_l - \varpi_l)\tilde{p}_m^*(q_m - \varpi_m)\tilde{p}_j(q_j - \varpi_j)\tilde{p}_k(q_k - \varpi_k)\rangle = \langle \tilde{p}_l^*(q_l - \varpi_l)\tilde{p}_j(q_j - \varpi_j)\rangle\langle \tilde{p}_m^*(q_m - \varpi_m)\tilde{p}_k(q_k - \varpi_k)\rangle + \langle \tilde{p}_l^*(q_l - \varpi_l)\tilde{p}_k(q_k - \varpi_k)\rangle\langle \tilde{p}_m^*(q_m - \varpi_m)\tilde{p}_j(q_j - \varpi_j)\rangle. \tag{6}$$

[4]It should be noted that the p's do not have a Fourier transform in the usual sense because they extend over all time. However, Wiener [14] showed through generalized harmonic analysis that the ''transform'' of the p's does in fact have meaning.

Given that the noise functions of the c individual component fields are mutually uncorrelated and that for every pair correlator involving one component field the frequencies in that pair correlator are δ-function correlated [12] due to stationarity of the p's, one writes

$$\langle \tilde{p}_j^*(a)\tilde{p}_k(b)\rangle = J_j^*(a)\,\delta(a-b)\,\delta_{jk} = J_k(b)\,\delta(b-a)\,\delta_{jk}, \tag{7}$$

where $J_{j,(k)}$ is the intensity level spectral density of the $p_{j(k)}$ and the Kronecker δ function, δ_{jk} forbids any correlation between colors indexed by j and k (for all $j \neq k$). With Eq. (7), Eq. (6) becomes

$$\begin{aligned}\langle \tilde{p}_l^*(q_k-\varpi_l)\tilde{p}_m^*(q_m-\varpi_m)\tilde{p}_j(q_j-\varpi_j)\tilde{p}_k(q_k-\varpi_k)\rangle \\ = J_j(q_j-\varpi_j)\,\delta(q_j-q_l)J_k(q_k-\varpi_k)\,\delta(q_k-q_m)\,\delta_{jl}\delta_{km} \\ + J_k(q_k-\varpi_k)\,\delta(q_k-q_l)J_m^*(q_m-\varpi_m) \\ \times \delta(q_m-q_j)\,\delta_{mj}\delta_{lk}. \end{aligned} \tag{8}$$

The Kronecker δ functions serve to ''color-lock'' the component fields and reduce the four-fold sum in (5) to a twofold sum, however, leaving the four integrations over independent q variables, though now as two pairs, with partners distinguished by the accent. Thus for the first term in Eq. (8) one finds that $q_l \Rightarrow \dot{q}_j$, $q_m \Rightarrow \dot{q}_k$ and for the second term $q_m \Rightarrow \dot{q}_j$, $q_l \Rightarrow \dot{q}_k$. The Dirac δ functions serve to further ''frequency lock'' the intensity level (pair correlator) contributions of each frequency within each quasi-cw component light source. Inserting Eq. (8) into (5), absorbing the $\chi^2_{2\varpi}$ into the proportionality constant, and performing the two trivial $\dot{q}$ integrations one obtains

$$\begin{aligned} I_{\mathrm{FS}}(\tau) \propto \sum_j^c \sum_k^c I_j I_k \int_{-\infty}^{\infty} dq_j \int_{-\infty}^{\infty} dq_k [J_j(q_j-\varpi_j) \\ \times J_k(q_k-\varpi_k) + J_k(q_k-\varpi_k)J_j^*(q_j-\varpi_j) \\ \times e^{i(q_k-q_j)\tau}], \end{aligned} \tag{9}$$

where $I_{j(k)} \propto (E^0_{j(k)})^2$. The t dependence has vanished for these stationary fields.

1. The first term in (9)

The first term in (9) (defined as N) can be rewritten as

$$\begin{aligned} N &= \sum_j^c \sum_k^c I_j I_k \int_{-\infty}^{\infty} dq_j \int_{-\infty}^{\infty} dq_k J_j(q_j-\varpi_j)J_k(q_k-\varpi_k) \\ &= \left\{ \sum_j^c I_j \int_{-\infty}^{\infty} dq J_j(q-\varpi_j) \right\}^2. \end{aligned} \tag{10}$$

The subscript on the q has been dropped without loss of generality. Changing the order of summation and integration one finds simply an integral over the intensity weighted composite spectrum, $\Sigma_j I_j J_j(q-\varpi_j)$. It contributes only to the τ-independent background.

2. The second term in (9)

The second term in brackets in (9) is τ dependent. Again the sums and integrals can be interchanged and written as

$$\begin{aligned} \sum_j^c \sum_k^c I_j I_k \int_{-\infty}^{\infty} dq_j J_j^*(q_j-\varpi_j) e^{-iq_j\tau} \\ \times \int_{-\infty}^{\infty} dq_k J_k(q_k-\varpi_k) e^{iq_k\tau} \\ = \left| \int_{-\infty}^{\infty} dq \sum_k^c I_k J_k(q-\varpi_k) e^{iq\tau} \right|^2, \end{aligned} \tag{11a}$$

where again the subscript on the q is dropped. Equation (11a) is just the mod-square of the Fourier transform of the same intensity weighted composite spectrum of the tailored light beam as in Eq. (10). This form will be picked up again in the Appendix where tailored beam interferometry is examined from a different point of view. A useful alternative expression for the sums and integrals over the second term in (9) is obtained with the change of variable $q'_{j,(k)} = q_{j,(k)} - \varpi_{j,(k)}$:

$$\begin{aligned} \sum_j^c \sum_k^c I_j I_k \int_{-\infty}^{\infty} dq_j J_j^*(q_j-\varpi_j) e^{-iq_j\tau} \int_{-\infty}^{\infty} dq_k J_k(q_k-\varpi_k) e^{iq_k\tau} \\ = \sum_j^c \sum_k^c I_j I_k e^{-i(\varpi_j-\varpi_k)\tau} \int_{-\infty}^{\infty} dq'_j J_j^*(q'_j) e^{-iq'_j\tau} \int_{-\infty}^{\infty} dq'_k J_k(q'_k) e^{iq'_k\tau}. \end{aligned} \tag{11b}$$

Equation (11b) will be used below for a tailored beam consisting of two-component Gaussian beams.

The sum of Eq. (10), as unity, and Eq. (11b) gives for the complete $I^{(2)}FS(2)$ interferogram

$$I_{FS}(\tau) \propto 1 + N^{-1} \sum_{j}^{c} \sum_{k}^{c} I_j I_k e^{-i(\varpi_j - \varpi_k)\tau} \int_{-\infty}^{\infty} dq_j' J_j^*(q_j') e^{-iq_j'\tau} \int_{-\infty}^{\infty} dq_k' J_k(q_k') e^{iq_k'\tau}. \tag{12}$$

Though this result is for an interferogram that is free of any consideration of unbalanced dispersion effects in the interferometer, the general aspects of the tailored light autocorrelation interferogram are seen. There are fringe patterns arising from the cross product of distinct component quasi-cw beams (the $e^{-i(\varpi_j - \varpi_k)\tau}$ factor). These are damped by the Fourier transforms of the component spectral densities to produce the envelope of the fringe pattern. An alternative formulation is presented in the Appendix in which the composite beam is treated as a single field having a complicated spectral density. The same results are obtained but now expressed in terms of the single composite spectrum rather than a weighted sum of component spectra. When this view is taken, there is a simple Fourier relationship between the composite spectrum and the autocorrelation trace. As seen in (A10) the *τ-dependent part* of the $I^{(2)}FS(2)$ interferogram is the mod-square of the Fourier transform of the composite spectral density.

B. Introduction of the effects of dispersion

With dispersive elements in the beam path(s) the bluer light components of the tailored field will suffer a greater phase lag than will the redder components. However, every pair correlator involves one field action each from F and F' and is frequency locked [Eq. (7)]. This implies that as long as the dispersive effects experienced for every frequency in F in one arm of the interferometer and the same frequency in F' in the other arm are exactly balanced, (12) can still serve as the proper expression for the $I^{(2)}FS(2)$ interferogram. Fully balanced dispersive effects assure that the two fields in each frequency-locked pair correlator experience the identical dispersion-induced delay. Thus the zero of the interferometric delay (τ) remains the same for each and every pair correlator with or without dispersion effects as long as these are exactly balanced between the F and F' arms and (12) holds. By contrast, ultrashort pulses are not immune to such dispersive effects (even when balanced) because the pulse is in fact temporally broadened (it is chirped) and this has drastic effects on its time resolution (the autocorrelation). In this sense the present tailored fields consisting of many colors of quasi-cw beams have an advantage.

However, as soon as the dispersive effects experienced by F and F' are not balanced new features arise. Now for any given color and frequency-locked pair correlator one field member (in F) of the pair correlator experiences a dispersion-induced delay that differs from its partner (in F') and hence requires a compensating offset in τ with respect to the peak for the case of balanced dispersion. The magnitude of this *difference* (the offset) is very dependent on the locked color involved in a given pair correlator. A single setting of τ can now no longer simultaneously maximize the individual interferograms stemming from a color j pair correlator and a color k pair correlator. This conflict not only leads to a reduction in the contrast ratio of the total $I^{(2)}FS(2)$ interferogram but also to curious changes in the fringe pattern. Alternatively, control over the relative phase lag between F and F' for each color can offer an interesting additional tool for tailoring the $I^{(2)}FS(2)$ interferogram. A simple realistic example is an interferometer having an effective thickness of quartz or glass that differs significantly (many mm to a few cm) between its two arms. Changing the thickness in one arm will control the degree of imbalance in the dispersion effects.

Unbalanced dispersion effects can be introduced into (12) simply by assigning to each component central frequency its own compensating offset at the delay line in F', τ_i for ϖ_i. (We shall assume for analytic convenience that this effect is constant over the bandwidth of each component color.) For exactly balanced dispersive effects the $\{\tau_i\}$ are all zero. Expression (12) now becomes

$$\begin{aligned} I_{FSd}(\tau) \propto 1 + N^{-1} \sum_{j}^{c} \sum_{k}^{c} I_j I_k e^{-i(\varpi_j - \varpi_k)\tau} e^{i\varpi_j\tau_j - \varpi_k\tau_k} \\ \times \int_{-\infty}^{\infty} dq_j' J_j^*(q_j') e^{-iq_j'(\tau - \tau_j)} \\ \times \int_{-\infty}^{\infty} dq_k' J_k(q_k') e^{+iq_k'(\tau - \tau_k)}, \end{aligned} \tag{13}$$

where the subscript d refers to the $I^{(2)}FS(2)$ signal subject to dispersion effects. Applications of (12) and (13) are now made in the context of a two-color tailored light field.

C. An example—a double Gaussian spectrum

As an example consider the tailored quasi-cw light source consisting of two Gaussians, one at a ''red'' carrier frequency ω_r and the other at a ''blue'' carrier frequency ω_b. The widths of these Gaussians are characterized by the parameters Γ_r and Γ_b, respectively. The intensity weighted composite spectral density is just

$$\begin{aligned} I_r J_r(q_r - \omega_r) + I_b J_b(q_b - \omega_b) \\ = A_r e^{-(q_j - \omega_r)^2/4\Gamma_r^2} + A_b e^{-(q_b - \omega b)^2/4\Gamma_b^2}, \end{aligned} \tag{14}$$

where the $A_{r,(b)}$ are constants such that this special composite spectral density (left-hand side) is normalized to unity. For this special two-color model (12) becomes

$$I_{\mathrm{FS}}(\tau)\propto 1+A_r^2e^{-2\Gamma_r^2\tau^2}+A_b^2e^{-2\Gamma_b^2\tau^2}+A_rA_be^{-\Gamma_r^2\tau^2-\Gamma_b^2\tau^2}[e^{-i\Delta_{br}\tau}+e^{i\Delta_{br}\tau}], \quad (15)$$

where $\Delta_{br}\equiv\omega_b-\omega_r$. And for the special case where $A_\tau=A_b=1/2$ and $\Gamma_r^2\simeq\Gamma_b^2=\Gamma^2$, (12) becomes simply

$$I_{\mathrm{FS}}(\tau)\propto 1+\tfrac{1}{2}e^{-2\Gamma^2\tau^2}[1+\cos\Delta_{br}\tau]. \quad (16)$$

Modified to include unbalanced dispersion effects [as per Eq. (13), Eq. (15) becomes

$$I_{\mathrm{FS}d}(\tau)\propto 1+A_r^2e^{-2\Gamma_r^2(\tau-\tau_r)^2}+A_b^2e^{-2\Gamma_b^2(\tau-\tau_b)^2}+A_rA_be^{-\Gamma_r^2(\tau-\tau_r)^2-\Gamma_b^2(\tau-\tau_b)^2}[e^{i\omega_b\tau_b-i\omega_r\tau_r}e^{-i\Delta_{br}\tau}+e^{-i\omega_b\tau_b+i\omega_r\tau_r}e^{i\Delta_{br}\tau}]. \quad (17)$$

Consider the difference between the blue-red offset, $\tau_{br}=\tau_b-\tau_r$, and set $\tau_r=0$ without loss of generality. Now $\tau_b=\tau_{br}$ and Eq. (17) becomes

$$I_{\mathrm{FS}d}(\tau)\propto 1+A_r^2e^{-2\Gamma_r^2(\tau)^2}+A_b^2e^{-2\Gamma_b^2(\tau-\tau_{br})^2}+A_rA_be^{-\Gamma_r^2(\tau)^2-\Gamma_b^2(\tau-\tau_{br})^2}[\cos(\omega_b\tau_{br})\cos\Delta_{br}\tau+\sin(\omega_b\tau_{br})\sin\Delta_{br}\tau]. \quad (18)$$

The robustness of the interferogram is very strongly dependent upon the stability of τ_{br}, because it appears with an optical frequency ω_b. Jitter in τ_{br} of more than ~ 1 fs would destroy the signal due to averaging the sine and cosine factors. Physically, τ_{br} corresponds to the separation of the peaks of the second and third terms of (18)—the separation between the red-only interferogram and the blue-only interferogram. Furthermore the fluctuations in τ_{br} require *frequency-dependent* fluctuations (otherwise τ_{br} cannot change), which may be due to, for example, unbalanced density (thermal) fluctuations in air or the optics between the two arms of the Michelson interferometer. These are apparently of very minor significance as is evident from the robust experimental $\mathrm{I}^{(2)}\mathrm{FS}(2)$ interferograms seen in the present experiment.

To illustrate, Fig. 1 shows plots of $\mathrm{I}_d^{(2)}\mathrm{FS}(2)$ interferograms [(18) with $\Gamma_b\simeq\Gamma_r\equiv\Gamma$] in terms of reduced variables ($x=\Gamma\tau$, $x_{br}=\Gamma\tau_{br}$, $w_{r,(b)}=\omega_{r,(b)}/\Gamma$) for six different values of the reduced offset imbalance x_{br}. It is noticed that as x_{br} increases, the peak-to-background contrast ratio of the interferograms diminishes, as anticipated. Interestingly, the phase of the fringe beating also changes sensitively to produce a variety of interferograms including asymmetric ones.

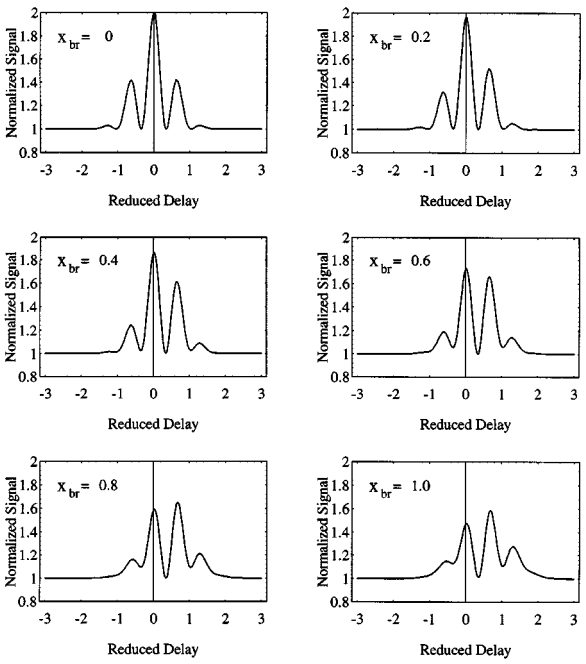

FIG. 1. Interferograms from (18) in reduced form plotted for several values of the reduced blue-red offset parameter, x_{br}, that expresses the unbalance dispersion effects between the two arms of the Michelson interferometer. The reduced Δ_{br} was chosen to be 1.44. At $x_{br}=0$ the interferogram has a peak-to-background contrast ratio of 2:1 and it is symmetric. As x_{br} increases the contrast ratio is reduced and the interferograms acquire an asymmetric structure. When the offset is roughly equal to the autocorrelation time of a noisy quasi-cw component field $x_{br}=1$ and the lower right panel is obtained.

III. EXPERIMENT

A general double noisy beam noncollinear $\mathrm{I}^{(2)}\mathrm{FS}(2)$ experiment consists of two dye lasers pumped by a single Nd:YAG laser each operating at zeroth-order diffraction such that much of the emission spectrum of the dye is emitted from the cavity. The two separate beams are made collinear to form a new beam having the composite spectral density of the two dye sources. The composite beam is now used in exactly the same manner as would be a noisy beam from a single source in noisy light experiments [1]. Briefly, the beam is sent through a Michelson interferometer. Emerging from the interferometer are twin parallel beams (F and F'), each having the identical composite spectral density but with F' in one arm having been delayed relative to F in the other arm by a variable delay τ. These beams, with distinct k vectors, are focused into a doubling crystal (KDP, for example). The beams (fundamental and summed frequencies) that exit the crystal are coarsely spectrally filtered to block the fundamentals and spatially filtered to isolate only those summed frequencies derived from a single action by each of F and F' in the second-order process (noncollinear frequency summing). The general setup is shown in Fig. 2.

The two dye lasers (Spectra Physics), PDL1 and PDL2, are operated at zeroth-order diffraction and pumped at 10 Hz by the same Nd:YAG laser (Spectra Physics). PDL1 initially contains rhodamine 590 ($\lambda_{\max}\sim 561$ nm) in MeOH; PDL2 contains rhodamine 610 ($\lambda_{\max}\sim 580$ nm) in MeOH (both dyes from Exciton). The resulting beams are combined by a beam splitter (bs1 in Fig. 2). The composite beam is first propagated 22 m past the interferometer to confirm that the beams are effectively collinear—to within less than 2×10^{-4} rad. Once such collinearity is achieved the composite beam (no longer propagated 22 m) is then sent directly into the Michelson interferometer to produce twin parallel beams (F and F'). F' is delayed with respect to F by a retroreflecting mirror mounted on a dc actuator (Control Techniques) that is computer controlled. $A\sim 1$ cm single

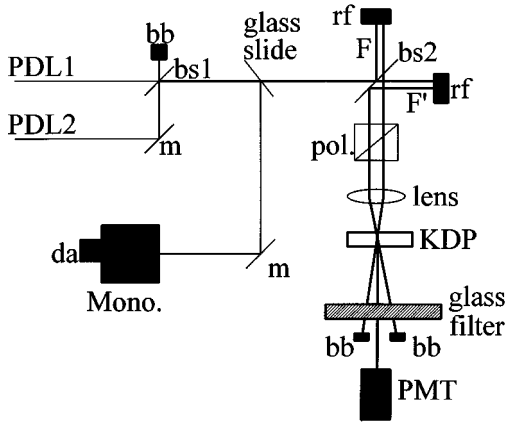

FIG. 2. A schematic of the experimental setup. The component beams from separated sources (PDL1 and PDL2) are combined at the beam splitter labeled bs1 to form a composite beam. The spectrum of this beam is obtained by picking off a small fraction and directing it into a monochromator and detecting with a diode array. The composite beam is split into twin beams F and F' and a relative delay τ is introduced by a computer controlled Michelson interferometer. These twin beams emerge parallel (but not collinear) from the interferometer and are focused into a KDP crystal. The FS(2) signal is coarsely spatially and spectrally filtered and detected using a photomultiplier tube (PMT). Mirror (m), beamsplitter (bs), retroreflecting mirror (rf), beam block (bb), polarizer (pol.), monochromator (Mono.), diode array (da).

sided beam splitter was used in the Michelson interferometer.[5] This introduces the major source of unbalanced dispersion effects measured by the relative blue-red off-set time τ_{br}. The parallel (but not collinear) beams F and F' are sent through a cubic polarizer and into an 18-cm focal length achromatic lens, which focuses the beams with approximate k vectors $\mathbf{k}$ and $\mathbf{k}'$ into a 1-mm-thick KDP crystal (Cleveland Crystal). The fundamentals and the frequency sum signals emerge as shown in Fig. 2. The former are blocked by a 7-54 Corning glass filter; an iris is used to somewhat broadly spatially select the desired $I^{(2)}FS(2)$ signal along $\mathbf{k}_s \simeq \mathbf{k}+\mathbf{k}'$. The signal is white detected by a photomultiplier tube and converted to a digital input where averaging over a number of shots (usually 10) is done by a home written data-acquisition program.

The power of each component of the composite beam is measured at the sample position by alternately blocking the output from PDL1 and PDL2 and is equalized through the use of a neutral density filter in the path of the appropriate PDL output. Since the composite beam embraces a frequency range of $\sim 500\ \mathrm{cm}^{-1}$, a single orientation of the KDP crystal cannot optimize the second-harmonic generation (SHG) of each of the component beams simultaneously. Instead the crystal is tuned to achieve equal SHG from each

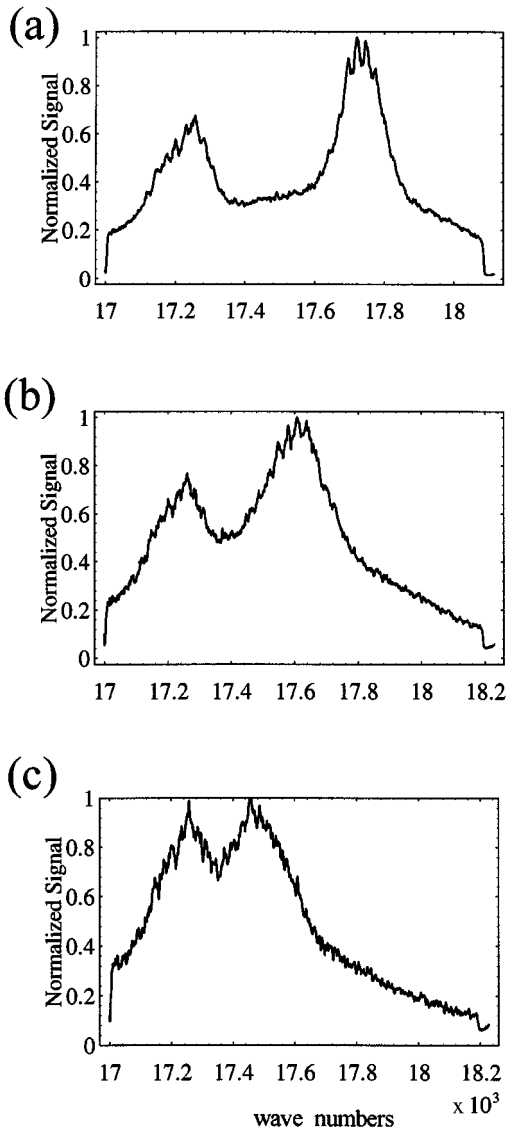

FIG. 3. The raw spectra for the tailored beam used in the experiment. To reduce Δ_{br} (top to bottom) small amounts of rhodamine 610 were successively added to the dye reservoir of PDL1, which originally contained only rhodamine 590. PDL2 contains only rhodamine 610 and is not changed. The two-color composite beam is constructed of these spectra after making both components of equal intensity by using a neutral density filter to achieve equal $I^{(2)}SHG(2)$ signal from each color alone. The separation of the peaks, $|\Delta_{br}|$ are (a) $\sim 400\ \mathrm{cm}^{-1}$, (b) $\sim 220\ \mathrm{cm}^{-1}$, and (c) $\sim 170\ \mathrm{cm}^{-1}$.

PDL individually. That is, the selected phase-matching angle is between the optimum angles for doubling rhodamine 590 and rhodamine 610. The above conditions effectively set $A_r = A_b$ in (13) and (18).

The separation of the two peak frequencies in the composite source can be reduced by mixing into the rhodamine 590 in PDL1 a small amount of rhodamine 610. This moves the peak frequency of PDL1 to the red—towards that of PDL2. Sequential additions of rhodamine 610 are made and $I^{(2)}FS(2)$ interferograms collected until the spectral peak of PDL1 is coincident with the rhodamine 610 peak of PDL2. The spectra of composite beams are obtained by picking off

[5]The geometry is such that in one arm of the interferometer F' trasverses the beam splitter (45° angle of incidence) three times while in the other arm F traverses it only once. The net effect is that F' travels through roughly 2.8 cm more quartz than does F. For example, the unbalanced dispersion effects for the case of quartz where the ''blue'' field is 560 nm and the ''red'' field is 580 nm is to make $\tau_{br} \sim 90$ fs [15].

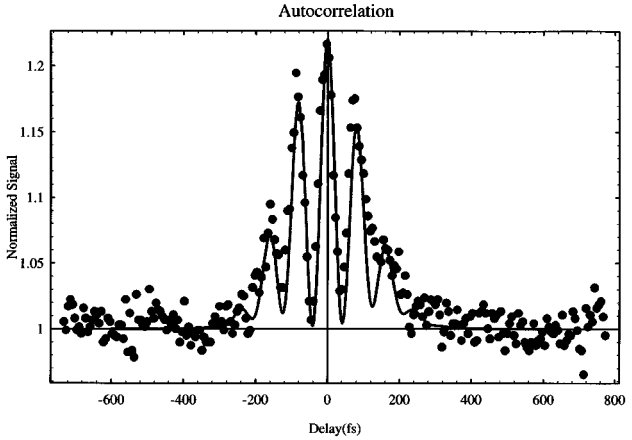

FIG. 4. $I^{(2)}FS(2)$ interferogram: experiment (dots), and theory (18) (line). The parameters are $\tau_{br}=112$ fs, $\Gamma_r=5.41\times10^{12}$ s^{-1}, $\Gamma_b=5.00\times10^{12}$ s^{-1}, $\tilde{\Delta}_{br}=401$ cm^{-1}, and scaling factor of the τ-dependent expression of (18) was 0.33.

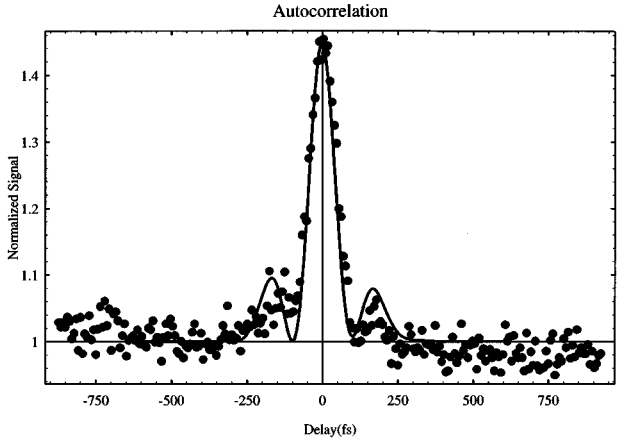

FIG. 6. $I^{(2)}FS(2)$ interferogram: experiment (dots), and theory [(18)] (line). The parameters are $\tau_{br}=45$ fs, $\Gamma_r=5.55\times10^{12}$ s^{-1}, $\Gamma_b=4.55\times10^{12}$ s^{-1}, $\tilde{\Delta}_{br}=167$ cm^{-1}, and scaling factor was 0.54.

a small fraction after bs1 (Fig. 2) using a glass microscope slide. This is directed into a SPEX triple monochromator and detected by a diode array (EG&G). The raw spectra of three such composite beams are shown in Fig. 3. The individual (PDL1 or PDL2 only) $I^{(2)}$SHG interferograms were separately recorded prior to the $I^{(2)}FS(2)$ signal from each composite spectrum. The relative offset (peak separation) between the individual $I^{(2)}$SHG interferograms was noted and used as a fitting parameter. The experimental τ_{br} ranged from over 100 fs to less than 50 fs as the Δ_{br} is diminished. (The values used in fitting the data are given in the legends of Figs. 4–6.)

IV. RESULTS AND DISCUSSION

It is shown experimentally how one can construct complex temporal probes by combining the output of separate dye lasers each operating in a broadband mode. Figures 4, 5, and 6 show different temporal probes [as $I^{(2)}FS(2)$ interferograms] provided by three different two-color composite sources formed as increasing amounts of rhodamine 610 are added to PDL1. In each case the right-hand side of Eq. (18) with $A_r=A_b=1/2$ is used to fit the data. The ω_b and Δ_{br} parameters come from the composite spectrum (Fig. 3) and $\Gamma_{r,(b)}$, τ_{br} are obtained from the individual (PDL1 or PDL2 only) $I^{(2)}$SHG interferograms. The spectral peak separation $\tilde{\Delta}_{br}$ (the circular frequency Δ_{br} is expressed in wave numbers $\tilde{\Delta}_{br}$) of the PDL1 and PDL2 beams decreases from ~400 cm^{-1} in Fig. 4 to the ~170 cm^{-1} in Fig. 6. The parameters are listed in the captions of the respective figures. The significant role of the unbalanced dispersive effects is evident (cf. Fig. 1) where the contrast ratio is seen to diminish and the symmetry of the interferogram is destroyed.

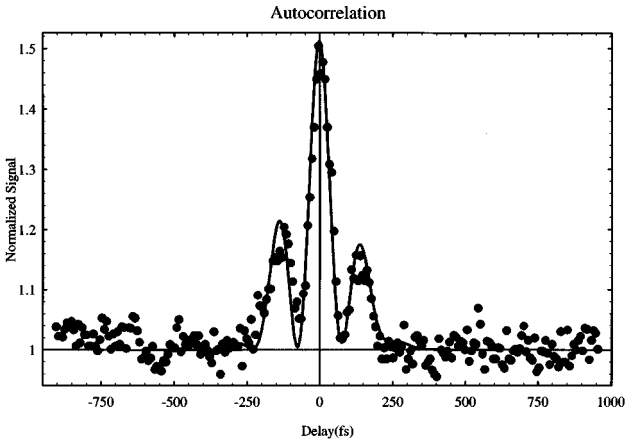

FIG. 5. $I^{(2)}FS(2)$ interferogram: experiment (dots), and theory [(18)] (line). The parameters are $\tau_{br}=74$ fs, $\Gamma_r=5.41\times10^{12}$ s^{-1}, $\Gamma_b=4.55\times10^{12}$ s^{-1}, $\tilde{\Delta}_{br}=217$ cm^{-1}, and scaling factor was 0.67.

Across Figs. 4–6 the interferometric time resolution of the fringe pattern is better (less than 100 fs in the case of Fig. 4) than that of either one of the component beams that have interferometric time resolution similar to that of the envelope of these fringes ($\sim$180–200 fs).

Basic aspects of Fourier transform theory are manifest in this experiment. The separation of the spectral peaks determines the period of the fringes seen in the temporal domain, with large separations yielding shorter oscillation periods. The spectral width (controlled by the widest of the two component spectra) determines the temporal ''envelope.'' Further, when the two Gaussian components have different widths the contrast in the fringes is reduced—their troughs do not reach the background level (see especially Figs. 4 and 6). The introduction of unbalanced dispersion effects adds another experimental parameter that may be used to construct a wider variety of interferograms. Asymmetrical traces can also be obtained when unbalanced dispersion effects are included as seen in Fig. 1and is evident from the experimental data (Figs. 4–6). When the dispersion effects felt by F and F' are balanced, the $I^{(2)}FS(2)$ interferograms must be symmetric, a point that remains to be demonstrated.

It must be mentioned that the peak-to-background ratio of these observed $I^{(2)}FS(2)$ interferograms is significantly less than 2:1. With balanced dispersion effects, theory requires a 2:1 peak-to-background contrast ratio [Eq. (12)—$(IFS)(\tau)=2$ for $\tau=0$ and 1 for $\tau\rightarrow\infty$]. In theory unbalanced dispersion can reduce the contrast ratio to as low as 1.25:1 as an extreme ($x_{br}\gg1$). This reduction of peak-to-background

contrast ratio with increasing differential offset is evident in the series of six reduced interferograms shown in Fig. 1. However, unbalanced dispersion effects cannot quite account for all of the experimental deviation from the 2:1 ideal ratio. In the experiments a general trend is noticed where, as the spectra of the two dye lasers move closer (diminishing τ_{br}), the contrast ratio strengthens (see Figs. 4–6). This is qualitatively consistent with the effects of unbalanced dispersion. But in general any imperfections in the experiment (scatter, etc.) are in any case strongly biased towards lowering the contrast ratio. Other noisy light experiments that have been performed with the same lasers show a correlation in the light fields that decays on a time scale of tens of picoseconds corresponding to the coherence time of the Nd:YAG pump laser. On the femtosecond time scale, this slow correlation decay manifests itself by contributing to the apparently τ-independent background signal. The actual contrast ratio would then be greater than that which is observed in an interferogram limited to only a few hundred femtoseconds. For these various reasons we have chosen simply to scale the magnitude of the τ-dependent term in (18) in order to best fit each of the observed $\mathrm{I}_d^{(2)}\mathrm{FS}(2)$ interferograms.

V. CONCLUSION

In the ultrashort pulse area of study, efforts have been made to shape the pulse envelope through phase or amplitude modulation [7–9]. Here it has been shown how a single noisy beam can be constructed of two (or more) quasi-cw light sources to produce complex $\mathrm{I}^{(2)}\mathrm{FS}(2)$ interferograms whose fringes offer the potential for constructing tailored temporal probes and obtaining shorter time resolution than available from a single noisy light source. This appears to be the quasi-cw light analog of amplitude modulation pulse shaping. One advantage of the composite light is that the available spectral domain likely exceeds that for short pulses. In principle one could combine nontransform limited sources of any color and in fact combine any number of beams which could lead to extremely short autocorrelation times and interesting tailored autocorrelation traces. In addition, the controlled introduction of unbalanced dispersion effects into the interferometer offers yet another adjustable parameter of potential use in constructing particular autocorrelation profiles. A practical complication for any source having a broad spectral range is obtaining a clean focus. Also, for phase-matched spectroscopies, simultaneous phase matching for all the colors contained in the beam is unlikely. This would be less of a problem for the (nearly) degenerate wave mixing spectroscopies such as coherent Raman scattering, photon echoes, etc., than for frequency summing, since in those cases the signal frequency approaches that of the input frequencies. Nonetheless, this composite light source may have applications in wave-packet production and control. The lack of cross-color coherence for noisy light (noisy light correlators are color locked) is complementary to the phase-locked nature of coherent femtosecond pulses and is of fundamental importance in the types of wave packets produced in a given experiment. More complicated temporal probes and wave packets could serve as elegant tools in areas of photophysics and nonlinear optics where wave-packet dynamics is of interest [8,10], such as in the study of solvent-system interactions in the condensed phase and the dynamics of customized intrachromophore wave packets. Additionally, tailored light probes are of interest in studying and controlling photochemical reactions where complicated driving functions determined from quantum-mechanical calculations have been shown (in simulations) to selectively emphasize particular reaction pathways [8,11]. We regard as the more immediate challenge the application of these quasi-cw tailored light sources to the various interferometric spectroscopies where quasi-cw (simple) noisy light had its beginning.

ACKNOWLEDGMENTS

We are grateful to Michael Stimson for his discussion of pulse shaping in the ultrafast arena. His discussion provided the impetus for this paper. D.J.U. also acknowledges Eric Parker for general advice regarding the experimental procedures. We gratefully acknowledge NSF Grant No. CHE-9311959 for support of this work.

APPENDIX: AN ALTERNATIVE FORMULATION OF THE $\mathrm{I}^{(2)}\mathrm{FS}(2)$ SIGNAL

In the text the tailored spectrum was built explicitly of multicolor component beams each having a simple Gaussian distribution. In this Appendix the tailored light source is viewed as a single quasi-cw source with a complicated spectral density having a single nominal carrier wave frequency $\boldsymbol{\varpi}$. (Let $\boldsymbol{\varpi}$ define some reference frequency in the spectrum of the tailored light source.) The results of the text can be obtained from such a viewpoint. The electric fields associated with F and F' are now just

$$E_F(t)=E_0p(t)e^{i\mathbf{k}\cdot\mathbf{r}-i\boldsymbol{\varpi}t}+\text{c.c.} \tag{A1}$$

and

$$E_{F'}(t)=E_0p(t-\tau)e^{i\mathbf{k}'\cdot\mathbf{r}-i\boldsymbol{\varpi}(t-\tau)}+\text{c.c.} \tag{A2}$$

Now p is a single complex stochastic function that carries the complex noise and obeys complex Gaussian statistics. It is assumed to be stationary and ergodic (on the femtosecond time scale). However, p does not have a simple noise Gaussian spectrum as the component color-dependent p_i's did in the text. The second-order phase-matched signal field for F and F' frequency summing that is launched by the polarization becomes

$$E_{2\boldsymbol{\varpi}}(t)\propto\chi_{2\boldsymbol{\varpi}}\int_{-\infty}^{\infty}dq\int_{-\infty}^{\infty}d\dot{q}\,\tilde{p}(q-\boldsymbol{\varpi})\tilde{p}(\dot{q}-\boldsymbol{\varpi})\times e^{-i(q+\dot{q})t}e^{i\dot{q}\tau}, \tag{A3}$$

where q and $\dot{q}$ are independent dummy frequency variables centered about $\boldsymbol{\varpi}$. The $\mathrm{I}^{(2)}\mathrm{FS}(2)$ signal is detected (and stochastically averaged) at the intensity level. The frequency summing intensity is

$$I_{\mathrm{FS}}(\tau,t)\propto\langle E^{*}_{2\varpi}(\tau,t)E_{2\varpi}(\tau,t)\rangle$$
$$\propto\chi^{2}_{2\varpi}\int_{-\infty}^{\infty}dq'\int_{-\infty}^{\infty}d\dot{q}'\int_{-\infty}^{\infty}dq\int_{-\infty}^{\infty}d\dot{q}$$
$$\times e^{-i(q+\dot{q}-\dot{q}-\dot{q}')t}$$
$$\times\langle\tilde{p}^{*}(q'-\varpi)\tilde{p}^{*}(\dot{q}'-\varpi)\tilde{p}(q-\varpi)\tilde{p}(\dot{q}-\varpi)\rangle$$
$$\times e^{-i(\dot{q}'-\dot{q})\tau}. \tag{A4}$$

Since p obeys complex Gaussian statistics, the four-point correlator can be factored into pair correlators:

$$\langle\tilde{p}^{*}(q'-\varpi)\tilde{p}^{*}(\dot{q}'-\varpi)\tilde{p}(q-\varpi)\tilde{p}(\dot{q}-\varpi)\rangle$$
$$=[\langle\tilde{p}^{*}(q'-\varpi)\tilde{p}(q-\varpi)\rangle\langle\tilde{p}^{*}(\dot{q}'-\varpi)\tilde{p}(\dot{q}-\varpi)\rangle$$
$$+\langle\tilde{p}^{*}(q'-\varpi)\tilde{p}(\dot{q}-\varpi)\rangle\langle\tilde{p}^{*}(\dot{q}'-\varpi)\tilde{p}(q-\varpi)\rangle]. \tag{A5}$$

Due to stationarity the frequency are δ-function correlated, allowing Eq. (A5) to be written as

$$\langle\tilde{p}^{*}(q'-\varpi)\tilde{p}^{*}(\dot{q}'-\varpi)\tilde{p}(q-\varpi)\tilde{p}(\dot{q}-\varpi)\rangle$$
$$=[J^{*}(q'-\varpi)\delta(q'-q)J(\dot{q}-\varpi)\delta(\dot{q}-\dot{q}')$$
$$+J^{*}(q'-\varpi)\delta(q'-\dot{q})J(q-\varpi)\delta(q-\dot{q}')]. \tag{A6}$$

Substituting this into (A4) and performing the two trivial integrations one obtains

$$I_{\mathrm{FS}}(\tau)\propto\int_{-\infty}^{\infty}dq\int_{-\infty}^{\infty}d\dot{q}[J^{*}(q-\varpi)J(\dot{q}-\varpi)$$
$$+J^{*}(\dot{q}-\varpi)J(q-\varpi)e^{-i(q-\dot{q})\tau}]. \tag{A7}$$

The first term in brackets is unity for normalized spectral densities and contributes only to the τ-independent background. The second term in brackets is τ dependent. The integrals can be separated and written as

$$\int_{-\infty}^{\infty}dqJ(q)e^{-iq\tau}e^{-i\varpi\tau}\int_{-\infty}^{\infty}d\dot{q}J^{*}(\dot{q})e^{i\dot{q}\tau}e^{-i\varpi\tau}$$
$$=\left|\int_{-\infty}^{\infty}dqJ(q)e^{-iq\tau}\right|^{2}, \tag{A8}$$

where the change of variable $q+\varpi\Rightarrow q'$ has been made in the first line, followed by $q'\Rightarrow q$ in the second line. Now, by the familiar Wiener-Khintchine theorem [12]

$$\int_{-\infty}^{\infty}dqJ(q)e^{-iq\tau}=\langle p(\tau)p^{*}(0)\rangle. \tag{A9}$$

We finally obtain

$$I_{\mathrm{FS}}(\tau)\propto 1+\left\{\frac{|\langle p(\tau)p^{*}(0)\rangle|^{2}}{\left|\int_{-\infty}^{\infty}J(q)e^{-iq\tau}dq\right|^{2}}\right. . \tag{A10}$$

That is, the τ-dependent part of the autocorrelation is determined by the mod-square of the Fourier transform of the spectrum of the tailored light. Equation (11a) can be put in this form by simply defining $J(q-\varpi)$ as the intensity weighted composite spectrum $(\Sigma_j^c I_j J_j)$

$$\left|\int_{-\infty}^{\infty}dq\sum_{j}^{c}I_jJ_j(q-\varpi_j)e^{-iq\tau}\right|^{2}=\left|e^{i\varpi\tau}\int_{-\infty}^{\infty}J(q)e^{-iq\tau}dq\right|^{2}, \tag{A11}$$

which again by the Wiener-Khintchine theorem puts (12) in the form of (A10).

The results for the double Gaussian example can be recovered via (A10) by realizing that the Fourier transform of the sum of two Gaussian is also a sum of two Gaussians but with associated oscillations of $e^{i\omega_r\tau}$ and $e^{i\omega_b\tau}$, respectively

$$e^{i\varpi\tau}\int_{-\infty}^{\infty}dqJ(q)e^{iq\tau}=A_re^{-\Gamma_r^2\tau^2}e^{i\omega_r\tau}+A_be^{-\Gamma_b^2\tau^2}e^{i\omega_b\tau}. \tag{A12}$$

Introducing the mod-square of Eq. (A12) into (A10) yields

$$I_{\mathrm{FS}}(\tau)\propto 1+A_r^2e^{-2\Gamma_r^2\tau^2}+A_b^2e^{-2\Gamma_b^2\tau^2}$$
$$+A_rA_be^{-\Gamma_r^2\tau^2-\Gamma_b^2\tau^2}[e^{-i\Delta_{br}\tau}+e^{i\Delta_{br}\tau}], \tag{A13}$$

where $\Delta_{br}\equiv\omega_b-\omega_r$. Expression (15) is recovered exactly. The $A_r=A_b=1/2$ and $\Gamma_r^2\simeq\Gamma_b^2=\Gamma^2$, (16) is also recovered, as is (18) after introducing the unbalanced dispersion effects.

[1] N. Morita and T. Yajima, Phys. Rev. A **30**, 2525 (1984); S. Asaka, H. Nakatsuka, M. Fujiwara, and M. Matsuoka, *ibid.* **29**, 2286 (1984); R. Beach and S. R. Hartmann, Phys. Rev. Lett. **53**, 663 (1984).

[2] A. C. Albrecht *et al.*, Laser Phys. **5**, 667 (1995); D. J. Ulness and A. C. Albrecht, in *Proceedings of the Fifteenth International Conference on Raman Spectroscopy*, edited by S. A. Asher and P. Stein (Wiley, New York, 1996).

[3] D. J. Ulness and A. C. Albrecht, Phys. Rev. A **53**, 1081 (1996).

[4] M. A. Dugan and A. C. Albrecht, Phys. Rev. A **43**, 3922 (1991).

[5] T. Kobayashi, Adv. Chem. Phys. **85**, 55 (1994).

[6] D. J. Ulness and A. C. Albrecht, in *Proceedings of the Fifteenth International Conference on Raman Spectroscopy* (Ref. [2]); M. J. Stimson, D. J. Ulness, and A. C. Albrecht (unpublished).

[7] J. P. Heritage, A. M. Weiner, and R. N. Thurston, Opt. Lett. **10**, 609 (1985); A. M. Weiner, J. P. Heritage, and E. M. Kirschner, J. Opt. Soc. Am. B **5**, 1563 (1988).

[8] G. R. Fleming (unpublished).

[9] A. M. Weiner, D. E. Leaird, J. S. Patel, and J. R. Wullert, Opt. Lett. **15**, 326 (1990); M. M. Wefers and K. A. Nelson, *ibid.* **18**, 2032 (1993); **20**, 1047 (1993).

[10] N. F. Scherer, A. J. Ruggiero, M. Du, and G. R. Fleming, J. Chem. Phys. **93**, 856 (1990).

[11] M. Messina, K. R. Wilson, and J. L. Krause, J. Chem. Phys. **104**, 173 (1996).

[12] L. Mandel and E. Wolf, *Optical Coherence and Quantum Optics* (Cambridge University Press, Cambridge, 1990); J. W. Goodman, *Statistical Optics* (Wiley, New York, 1985).

[13] P. N. Butcher and D. Cotter, *The Elements of Nonlinear Optics* (Cambridge University Press, Cambridge, 1990).

[14] N. Wiener, Acta Math. **55**, 117 (1930).

[15] The estimate was based on the dispersion formula for quartz given in W. J. Tropf, M. E. Thomas, and T. J. Harris, *The Handbook of Optics II*, edited by M. Bass *et al.* (McGraw-Hill, New York, 1995).